NeuroImage 125 (2016) 422–427

Contents lists available at ScienceDirect

NeuroImage

journal homepage: www.elsevier.com/locate/ynimg

Deep brain stimulation of the ventromedial prefrontal cortex causes reorganization of neuronal processes and vasculature

M. Mallar Chakravarty [a,b,c,*,1], Clement Hamani [e,f,1], Alonso Martinez-Canabal [g], Jacob Ellegood [h], Christine Laliberté [h], José N. Nobrega [d,f], Tejas Sankar [e,i], Andres M. Lozano [e], Paul W. Frankland [g,k,l,m], Jason P. Lerch [g,h,j]

[a] Cerebral Imaging Centre, Douglas Mental Health University Institute, Canada
[b] Department of Psychiatry, McGill University, Canada
[c] Department of Biomedical Engineering, McGill University, Canada
[d] Department of Psychiatry, University of Toronto, Canada
[e] Division of Neurosurgery, Toronto Western Hospital, Canada
[f] Behavioural Neurobiology Laboratory, Campbell Family Mental Health Research Institute, Centre for Addiction and Mental Health, Canada
[g] Program in Neuroscience and Mental Health, The Hospital for Sick Children, Canada
[h] Mouse Imaging Centre (MICe), The Hospital for Sick Children, Canada
[i] Division of Neurosurgery, University of Alberta, Canada
[j] Department of Medical Biophysics, University of Toronto, Canada
[k] Department of Psychology, University of Toronto, Toronto, Canada
[l] Department of Physiology, University of Toronto, Toronto, Canada
[m] Institute of Medical Science, University of Toronto, Toronto, Canada

ARTICLE INFO

Article history:
Received 27 March 2015
Accepted 18 October 2015
Available online 23 October 2015

ABSTRACT

Background: Chronic high-frequency electrical deep brain stimulation (DBS) of the subcallosal cingulate region is currently being investigated clinically as a therapy for treatment of refractory depression. Experimental DBS of the homologous region, the ventromedial prefrontal cortex (VMPFC), in rodent models has previously demonstrated anti-depressant-like effects. Our goal was to determine if structural remodeling accompanies the alterations of brain function previously observed as a result of chronic DBS.

Methods: Here we applied 6 h of high-frequency bilateral VMPFC DBS daily to 8 9-week old C57Bl/6 mice for 5 days. We investigated the "micro-lesion" effect by using a sham stimulation group (8 mice) and a control group (8 mice with a hole drilled into the skull only). Whole brain anatomy was investigated post-mortem using high-resolution magnetic resonance imaging and areas demonstrating volumetric expansion were further investigated using histology and immunohistochemistry.

Results: The DBS group demonstrated bilateral increases in whole hippocampus and the left thalamus volume compared to both sham and control groups. Local hippocampal and thalamic volume increases were also observed at the voxel-level; however these increases were observed in both DBS and sham groups. Follow-up immunohistochemistry in the hippocampus revealed DBS increased blood vessel size and synaptic density relative to the control group whereas the sham group demonstrated increased astrocyte size.

Conclusions: Our work demonstrates that DBS not only works by altering function with neural circuits, but also by structurally altering circuits at the cellular level. Neuroplastic alterations may play a role in mediating the clinical efficacy of DBS therapy.

Introduction

High-frequency deep brain stimulation (DBS) delivered using a neurosurgically implanted electrode has been applied with great clinical efficacy in the treatment of Parkinson's disease and other movement disorders (Limousin et al., 1995). Given the success of this treatment for movement disorders, the use of chronic DBS has been proposed as a treatment for several other neuropsychiatric conditions as a means of compensating for malfunctioning brain circuitry (Lozano and Lipsman, 2013). Recently, the subcallosal cingulate region has been used as a DBS target in treatment refractory depression (TRD) (Lozano et al., 2008; Mayberg et al., 2005), with patients receiving the therapy demonstrating sustained anti-depressant response in 3–6 year follow-

* Corresponding author at: Cerebral Imaging Centre, Douglas Mental Health University Institute, 6875 LaSalle Boulevard, Verdun, QC H4H 1R3, Canada.
E-mail address: mallar@cobralab.ca (M.M. Chakravarty).
[1] These two authors contributed equally to this work.

http://dx.doi.org/10.1016/j.neuroimage.2015.10.049
1053-8119/

up open label studies (Kennedy et al., 2011) in a clinical population at high-risk for suicide (Conwell and Brent, 1995). In patients with TRD, local and remote changes in brain function in response to the focal application of subcallosal DBS have been previously demonstrated and may account, in part, for the therapeutic mechanism of action of DBS in depression (Lozano et al., 2008; Mayberg et al., 2005). Experimental studies involving stimulation of the ventromedial prefrontal cortex (VMPFC; the rodent homologue of the subcallosal cingulate region) in normal wild-type rats demonstrate the alleviation of depressive-like behaviors due to being subjected to a forced swim test (Hamani et al., 2010, 2012). Recent findings from our group show that in addition to functional remodeling, DBS applied in the context of neuropsychiatric disorders may mediate clinical efficacy through neuroanatomical remodeling as well. For example, DBS applied to key nodes in the memory circuit of rodents (Laxton et al., 2010) (such as the entorhinal cortex and the anterior nucleus of the thalamus) induces the generation of new neurons that, once mature, integrate into hippocampal memory circuits responsible for the maintenance of memory (Hamani et al., 2011; Stone et al., 2011). There is mounting evidence that neuroanatomical reorganization is also occurring in patient populations being treated with DBS. In a recent clinical finding, two Alzheimer's disease patients demonstrated hippocampal growth and improvement in their clinical presentation in response to chronic administration of DBS to the fornix (Sankar et al., 2015).

However, in the context of TRD, it is unclear as to whether or not these changes in brain function and behavior are accompanied or mediated by neuroanatomical reorganization, and if so, in what part of the associated network remodeling occurs. There is also recent evidence that the microlesion caused by the implantation of the DBS electrode itself may account for some improvement in symptomatology. We do note, however, that the use of lesion-otomies has been previously proposed in the treatment of major depression, often with mixed results. These include lesions throughout the cingulate, the internal capsule, and the tracts adjacent to the caudate nucleus (Shah et al., 2008); therefore there may be a neuroanatomical basis for remodeling observed due to microlesions and we speculate that neuroanatomical remodeling may be further modulated by chronic deep brain stimulation (possibly leading to therapeutic efficacy). While the microlesion phenomenon has been receiving some attention in the Parkinson's disease literature (Borden et al., 2014; Le Goff et al., 2014; Maltete et al., 2008, 2009), it has been relatively understudied.

Given the emerging interest in the subcallosal cingulate with respect to other neuropsychiatric disorders, such as treatment-refractory anorexia nervosa (Lipsman et al., 2013), it is critical to determine whether and to what extent neuroanatomical remodeling, and more specifically, if changes in neuronal processes, glial cells, and vasculature occur in response to DBS of this region. In this manuscript, we tested this open question by applying DBS to the ventromedial prefrontal cortex (VMPFC; the rodent homologue to the human subcallosal cingulate (Hamani et al., 2010, 2012)) of 8 9-week-old male C57Bl/6 mice. We used whole-brain high-resolution magnetic resonance imaging (MRI) data to analyze the neuroanatomical effects on the stimulated groups. To test the micro-lesion effect we also analyzed the neuroanatomy of a group receiving sham stimulation (i.e., stimulator implanted but no active stimulation received). Volumetric changes observed using MRI analysis were then used to guide histological and immunohistochemical analyses.

Materials and methods

Surgeries, electrode implantation and deep brain stimulation

To test how DBS may impact neuroanatomical networks and brain-wide neuroanatomical remodeling we applied DBS to 8 C57Bl/6 mice (~25 g; Charles River, Wilmington, Massachusetts, USA; all males; 9 weeks old). Mice were anesthetized with ketamine/xylazine (75/10 mg/kg i.p.) and had their heads fixed to a stereotaxic frame (David Kopf Instruments; Tujunga, CA, USA). Electrodes with a diameter of 125 μm and a 0.5 mm^2 of exposed surface were connected to a plastic pedestal (Plastics One; Roanoke, VA, USA) and bilaterally implanted in the VMPFC (anteroposterior +1.7, lateral ±0.2, depth 1.2 mm) and used as cathodes (Franklin and Paxinos, 2004). A screw implanted over the somatosensory cortex was used as the anode. Two additional screws were attached to the skull for better securing the cap in place. Electrodes and screws were fixed to the skull with dental acrylic cement. A week after surgery, the DBS group received stimulation for 6 h a day over five days (similar to the design previously used from our group in the study of rats (Hamani et al., 2010, 2012); stimulation parameters: 50 μA, 130 Hz, 90 μs pulse width). These settings were selected as they have been previously effective in improving memory performance in the Morris water maze (Stone et al., 2011) and approximate those used in most clinical applications of DBS if the charge density is taken into account.

To test the influence of the so-called "micro-lesion effect", where symptom improvement is noted shortly after electrode implantation and before DBS has been delivered or optimized (Lozano et al., 2008; Mayberg et al., 2005; Cersosimo et al., 2009; Granziera et al., 2008), we studied an additional group (n = 8) receiving sham stimulation (i.e., where the stimulator is implanted and not turned on). A third control group of 8 mice had holes drilled in the skull but no electrodes implanted (total: 24 mice total, all same background strain, males, and age as the DBS group). The control group was handled over 5 days in order to mimic the handling of both sham and DBS groups.

Magnetic resonance imaging (MRI)

Three days after the end of stimulation mice were perfused through the *left* cardiac ventricle with 30 mL of phosphate-buffered saline (PBS) (pH 7.4) containing 2 mM of ProHance® (Bracco Diagnostics Inc., Princeton, NJ) at room temperature (25 °C). This was followed by infusion with 30 mL of 4% paraformaldehyde (PFA) and 2 mM of ProHance® (Bracco Diagnostics Inc., Princeton, NJ) in PBS at room temperature. Following perfusion, the heads were removed along with the skin, lower jaw, ears and the cartilaginous nose tip. The remaining skull structures containing the brain were allowed to postfix in 4% PFA and 2 mM of ProHance® at 4 °C for 12 h and was stored in this fashion for 72 h prior to imaging. A multi-channel 7.0 T MRI scanner (Agilent, Palo Alto, CA) was used to acquire anatomical images of brains within skulls (Nieman et al., 2007). Prior to imaging, the samples were removed from the contrast agent solution, blotted and placed into 13-mm-diameter plastic tubes filled with a proton-free susceptibility-matching fluid (Fluorinert FC-77, 3 M Corp., St. Paul, MN). An array of 16 custom built solenoid coils was used for high-throughput scanning of the specimens using a T2-weighted 3D Fast Spin Echo (FSE) sequence, with TR = 2000 ms, echo train length = 6, TE_{eff} = 42 ms, FOV of 25 mm × 28 mm × 14 mm, and a matrix size of 450 × 504 × 250. This yields an isotropic (3D) resolution of 56 μm. In the first phase encode dimension, consecutive k-space lines were assigned to alternating echoes to move discontinuity related ghosting artifacts to the edges of the FOV. This sequence involves oversampling in the phase encoding direction by a factor of 2 to avoid the interference of these artifacts. This FOV direction was subsequently cropped to 14 mm after reconstruction. Total imaging time was ~12 h.

Image processing for MRI data

Anatomical changes accompanying DBS were estimated using deformation-based analysis of the T2-weighted MRI data (as described in previous publications from our group (Lerch et al., 2008)). All image processing was carried out with images in minc format using the minc suite of software tools (http://www.bic.mni.mcgill.ca/ServicesSoftware/ServicesSoftwareMincToolKit). All MRI volumes were rigidly rotated and translated (3 rotations and 3 translations) to match an initial atlas. All possible pair-wise 12-parameter transformations (3 rotations, translations,

scales and shears) (Collins et al., 1994) were estimated and an average linear transformation was calculated for each image, thus effectively scaling each brain to the average size of the population. After applying the average transformation, MRI volumes were averaged in order to create a first population-based model. A multi-generation, multi-resolution fitting strategy was then initialized where each brain is nonlinearly registered using the ANTs algorithm (Avants et al., 2008), modified to work with MINC data (https://github.com/vfonov/ANTs) and for the mice brain (van Eede et al., 2013). Each mouse brain was nonlinearly registered to the 12-parameter population atlas, and subsequently to the atlas of the previous nonlinear registration. Three generations were estimated, as per previous work from our group (van Eede et al., 2013). The registration parameters at each stage have are detailed in Supplementary Table 1. The final deformation fields map each T2-weighted volume to the average of the entire population based on the minimum deformation required to map each subject to the average of the group (i.e., the so-called minimum deformation template). Using these final deformations, we customized an atlas containing 62 neuroanatomical areas to each of the mice in the study to enable the estimation of structure volume (Dorr et al., 2008). The log-transformed Jacobian determinant (Chung et al., 2001), a measure of local expansion and contraction, was estimated at each node in the final deformation fields. Statistical analysis was carried out using a voxel-by-voxel general linear model included in the RMINC package (https://wiki.phenogenomics.ca/display/MICePub/RMINC) and all results were corrected for multiple comparisons using the False Discovery Rate (Genovese et al., 2002). All mice were analyzed through the development of a single group-wise average to enable direct comparisons between all through of the groups. We have previously used this method to estimate neuroanatomical differences in response to different maze training strategies learned over 5 days (Lerch et al., 2011), a week of motor skills training (Scholz et al., 2015), or 24 h of environmental enrichment (Scholz et al., 2015), demonstrating that this method is sensitive to subtle neuroanatomical differences between mice.

Histological/immunohistochemical processing and imaging

50 μm sections were cut in a cryostat (Leica CM1850; Wetzlar, Germany) from regions of interest. Sucrose 30% in PBS was used to submerge the brains before slicing. The brain sections were stored in the freezer using 10% ethylene glycol and 40% glycerol in PBS.

Each sixth section was placed in a well with antifreezer solution (50% glycerol [Sigma; St. Louis, MO, USA], 10% ethylene glycol [Sigma] and kept at −20 °C until use. Sections were thoroughly washed and placed in citrate buffer (Sigma) pH 6.0 at 95 C during 1 h. After washed, the sections were blocked for peroxidase activity in 0.3% H_2O_2 during 30 min, later were blocked with normal goat serum 3%, bovine serum albumin 1.5% and Tx100 0.3% during 2 h. Sections were immediately transfer to the primary antibody. With all the primary antibodies used, sections were incubated at room temperature ON. After being thoroughly washed, some primary antibodies were detected directly with appropriate secondary fluorescent antibodies, mouse glial fibrillary acidic protein (GFAP; cell signaling, Danvers, MA, USA) was detected using antimouse-Alexa 568 (Invitrogen, Carlsbad, CA, USA); rabbit polyclonal anti-collagen IV (1:1000; Chemicon, Temecula, CA, USA) was detected using anti-rabbit Alexa 488. Rabbit Synaptophysin (Abcam, Cambridge, England, United Kingdom) was detected using biotynilated anti-rabbit (Jackson), followed by avidin biotin complex (Vector; Burlingame, CA, USA) and developed using bio-tyramide signal amplification kit (Invitrogen) and *streptavidin-horseradish peroxidase*-568 (Invitrogen). After color developing, all sections were placed in 4′,6-diamidino-2-phenylindole solution (DAPI; Sigma) during 20 min, washed again, mounted and coverslipped with permafluor (Thermo Scientific; Waltham, MA, USA).

For each antibody, slices were selected at 300 μm. After a series was selected for collagen, GFAP, and DAPI, the next series was selected for synaptophysin. For every antibody tested, we performed previous probes of staining without the antibody where no staining was shown besides the usual background commonly observed in fluorescent probes upon brain tissue. We also examined that the anatomic localization of the signal corresponded with previous literature. Finally, images of the structures were taken with 10× and 20× objectives of a microscope Olympus BX61 (Center Valley, PA, USA), with a Reiga camera 1100.

Histological/immunohistochemical image analysis

Digitized sections were analyzed using the open-source CellProfiler software (Carpenter et al., 2006). The following CellProfiler modules and parameters were used for GFAP and collagen: 1) unmix colors; 2) invert each separate color; 3) identify primary objects (astrocytes) with a typical diameter of 4–90 pixels using the Otsu method and with intensity to separate clumped objects; 4) identify primary objects (vessels) with a typical diameter of 10–400 pixels using the Otsu method and with intensity to separate clumped objects. For synaptophysin: 1) correct illumination using splines with 4 spline points; 2) convert to grayscale; 3) identify primary objects (DAPI) with a typical diameter of 6–30 pixels using the Otsu method; 4) mask the input image with the identified nuclei from the DAPI stain retaining everything outside of the nuclei; 5) rescale intensity to be between 0 and 1; and 6) measure image intensity.

Statistical analysis of histological data

All statistical analyses were carried out in R (http://www.r-project.org/). Comparisons between DBS, sham, and control groups were carried out using mixed-model regression as it permits the inclusion of multiple measurements per mouse (Pinheiro and Bates, 2000). Correlations between the histological data and the Jacobian determinant were performed using the mean value from the histological analysis described above. In cases where greater than three measurements for a single structure were available, a trimmed mean (removing the maximum and minimum values) was used.

Results

All images were successfully processed through the automated image processing pipeline detailed in Section 2.3. It is clear that the pipeline is able to handle discrepant morphology created by the DBS electrode (see Supplementary Materials Fig. 1). Since we expected artefactual volumetric expansion in the vicinity of the site where the electrode was inserted, we instead focused our analysis on volumetric expansions observed distal to this region.

After correcting for multiple comparisons for 62 structures using the False Discovery Rate (FDR) (Genovese et al., 2002), bilateral hippocampal volume was larger in the DBS group in comparison to both the sham (5% FDR, $t = 5.3$) and control groups (10% FDR, $t = 3.8$; see Fig. 1A, i). The volume of the left thalamus was also larger in the DBS group in comparison to both the sham (5% FDR, $t = 4.9$) and control (10% FDR, $t = 3.6$) groups. After images were analyzed for volumetric expansion at the voxel-level, we observed volumetric expansions in four specific locations that survived 5% FDR correction when comparing DBS and control groups: in the anterior portion of the left hippocampus ($t = 3.3$), bilaterally in the body of the hippocampus ($t = 3.0$ and $t = 2.8$; left and right respectively; see Fig. 1B, i), and in the anterior portion of the left thalamus ($t = 2.1$; see Fig. 1B, ii) in comparison to the control mice. Surprisingly, the sham group also demonstrated volumetric increase relative to controls in the same regions compared to controls ($t = 3.3$, $t = 3.0$, $t = 2.0$ for left anterior hippocampus and body of the hippocampus and the left anterior thalamus respectively; all surviving 5% FDR), although the absolute value of these volumetric increases do not translate to increased total hippocampal volume. Local volume changes showed higher variability in the sham group in comparison to the DBS group (Bartlett's $K^2 = 2.93$, $p = 0.086$ for hippocampus).

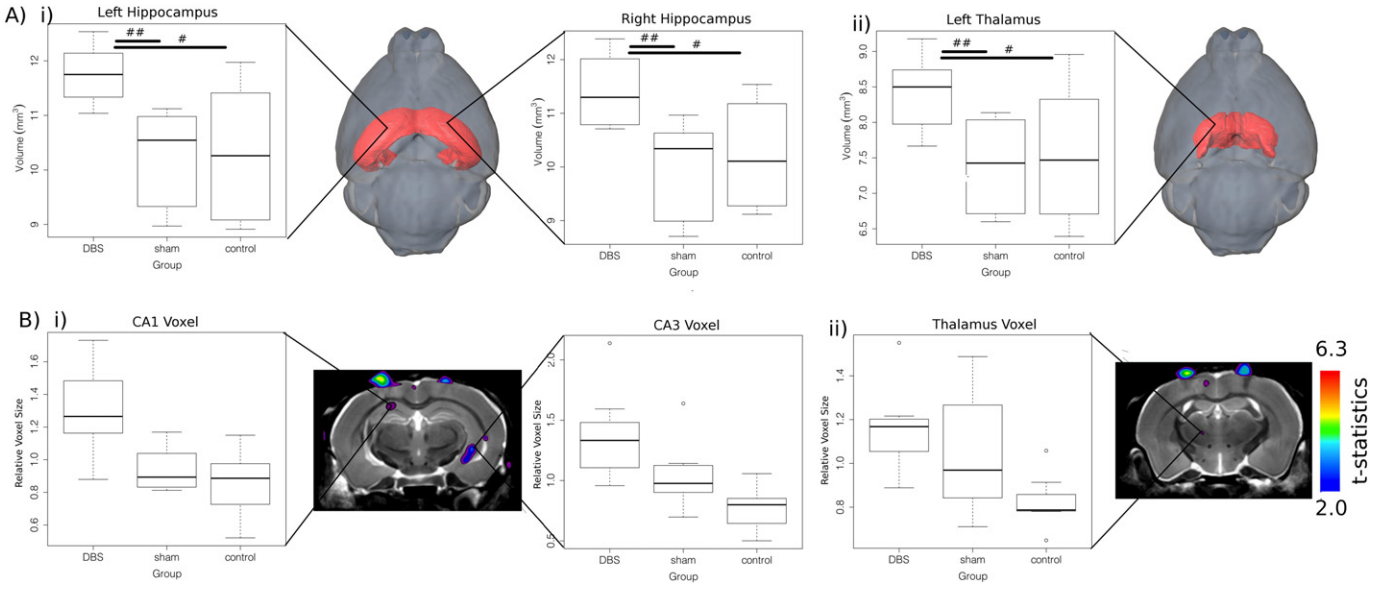

Fig. 1. A) Mice receiving DBS show larger i) bilateral hippocampus volume and ii) left thalamic volume. No volumetric differences were observed between sham and control groups at the whole structure level. B) These findings of overall volume increases can be localized to local volumetric expansions in both the i) hippocampus (bilaterally) and the ii) left thalamus. Note that open circles in B) represent individual data points that do not fall within the bounds of the box and whisker plots. Significant results that are observed in the superior margin of the brain are due to ground screws implanted for the DBS stimulator. # and ## denote survival of 10% and 5% false discovery rate correction.

Subsequent histological analysis in these regions demonstrated evidence of neuroanatomical remodeling. The DBS group showed increased hippocampal blood vessel diameter relative to controls (collagen, $t = 4.21$; $p < 0.001$; see Fig. 2A, ii). Synaptic density (synaptophysin) was increased relative to controls in both the DBS ($t = 3.18$; $p < 0.001$) and sham groups ($t = 2.86$; $p < 0.005$; see Fig. 2A, iv). In addition, there was evidence of increased astrocyte area in the hippocampus in the sham group compared to controls

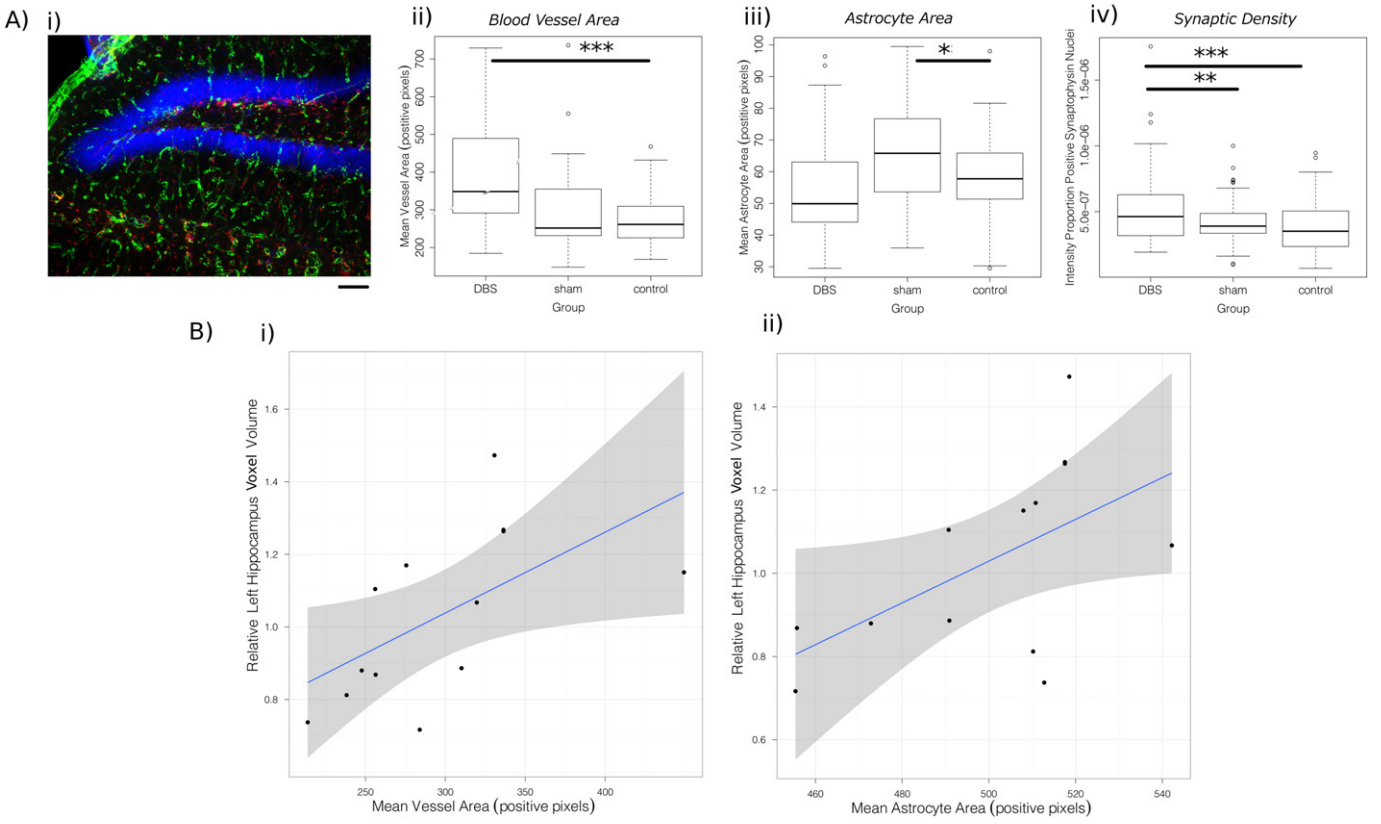

Fig. 2. A) Subsequent evaluation using histological preparations demonstrate that mice receiving DBS i) sample slide demonstrating a triple stained image using collagen (green), GFAP (red), and DAPI (blue) ii) have larger blood vessels (collagen stain), while the iii) sham group demonstrates larger astrocytes (GFAP stain). Mice receiving DBS also show iv) increased synaptic density (as measured using synaptophysin). B) Significant correlation of the i) mean vessel area and the ii) mean astrocyte area with the relative change in voxel volume was observed at the peak location of volumetric expansion in the hippocampus. Note that open circles in A) represent individual data points that do not fall within the bounds of the box and whisker plots. *, **, *** are statistically significant at $p < 0.05$, <0.005, and <0.001.

($t = 3.16$; $p < 0.005$; as measured using GFAP; see Fig. 2A, iii). Blood vessel ($t = 3.19$, $p < 0.05$, $R^2 = 0.28$) and astrocyte ($t = 2.24$, $p < 0.05$, $R^2 = 0.25$) size were well correlated with hippocampal volumetric expansion observed on MRI and accounted for the largest proportion of the overall variance in volume (see Fig. 2B).

Discussion

In this manuscript we demonstrate evidence that both the implantation of a DBS electrode and active simulation via DBS in the rodent homologue of the subcallosal cingulate region is associated with neuroanatomical remodeling at the level of the density of synaptic connections. We further demonstrate that active DBS may be involved in remodeling of the vascular architecture, resulting in increased blood vessel diameter. Traditionally, DBS has been considered a purely symptomatic therapy, unable to influence brain structure. However, these results, may be seen as complementary to other results from our group (Hamani et al., 2011; Stone et al., 2011). They demonstrate that both the insertion of the DBS electrode and active electrical stimulation may induce distinct and overlapping neuroanatomical remodeling at the cellular level. Importantly, these results also demonstrate that the neuroanatomical rearrangement in response to DBS can occur distal from (i.e., either upstream or downstream of) the stimulation site. In other words, DBS impacts components of neuroanatomical networks that are connected to the stimulation site through multiple synapses (Stone et al., 2011). Our observation of neuroanatomical rearrangement in both the hippocampus and the anterior thalamus in response to DBS of the VMPFC provides further support for this notion. In fact, further exploration using the Allen Institute Mouse Brain Connectivity Atlas (Oh et al., 2014) demonstrates connectivity between the VMPFC, the anterior portions of the thalamus, and hippocampal regions such as CA1 and CA3 (regions where volumetric expansion was found in our study using volumetric MRI; see Supplementary Figure S2).

Our results also suggest that neuroplasticity may be vital to the efficacy of DBS for depression and further suggest that the hippocampal growth observed may be necessary for providing an anti-depressant effect. While hippocampal decreases have previously been reported in TRD (McKinnon et al., 2009), there have been reports of 5% bilateral hippocampal growth in refractory patients as an acute response to electroconvulsive therapy (Nordanskog et al., 2010). Studies of depressed non-human primates have observed decreased neuropil and cell layer volumes in the CA1 and dentate gyrus regions of the hippocampus (Willard et al., 2013). Interestingly rat depression models treated with another form of brain stimulation, electroconvulsive seizure treatment, demonstrate an increased number of glial cells in the hilus of the hippocampus (Kaae et al., 2012) and an increase in the total number of synapses (Chen et al., 2009); this remodeling was also associated with antidepressant-like effects in these rats. Other preclinical studies also note specific alteration and increases in hippocampal volumes after the administration of anti-depressant medications (Venna et al., 2009); while some pharmacological treatments (such as imipramine) may modulate the establishment of new synaptic connections and may actually remodel existing synapses by increasing modulatory spine synapses and altering the normative distribution of spine to shaft synapsis (Chen et al., 2008).

Our results also demonstrate that neuroanatomical remodeling occurs even in response to a sham DBS insertion, suggesting that improvements seen clinically after DBS insertion (Cersosimo et al., 2009; Granziera et al., 2008) may not entirely be caused by a placebo effect. However, while both active and sham DBS cause increased synaptic density, there appears to be potential reactive gliosis (much like the effects previously reported in response to a needle insertion to the hippocampus (Song et al., 2013)) in response to the sham stimulator. It is possible that these mechanisms are being further modulated through active stimulation. While purely speculative, it is also possible that the sham group is experiencing the increase of neutrophic factors often seen in the mammalian brain in response to acute injury or lesions (Needels et al., 1985, 1986).

Our finding of increased collagen staining following VMPFC DBS leads us to speculate that the phenomenon of increased cerebral blood flow observed at 6 months in TRD patients receiving subcallosal DBS may be mediated by remodeling at the vascular level (Lozano et al., 2008). Interestingly, our findings and the findings from the initial clinical trials are at odds with measurements of blood flow in response to other forms of brain stimulation such as transcranial direct current stimulation in humans (Stagg et al., 2013) that demonstrate decreases in cortical perfusion as a result of both anodal and cathodal stimulations of the dorsolateral prefrontal cortex. Similarly, DBS of the rat hippocampus decreased hippocampal regional cerebral blood flow as evaluated by single photon emission computed tomography (Wyckhuys et al., 2010). Conversely, there is evidence of artery dilation as a result of focal electrical stimulation in the nucleus basalis of Meynert based on two-photon microscopy experiments; however this stimulation occurred at a lower frequency (50 Hz) (Hotta et al., 2013). Despite these conflicting previous results, there is little in the way of investigation between the coupling between DBS and alterations in vascular morphometry and arborization and alteration in the dynamics of cerebral blood flow. The differential effects described above suggest that any changes in cerebral blood flow mediated by brain stimulation may be dependent on the type of stimulation, the frequency of the stimulation, and the stimulation target. Clearly, further investigation along these lines is required to better understand the coupling between blood flow, vascular alterations, and the application of DBS.

Finally, there are limitations to consider in the interpretation of the results that are presented in this manuscript. Our work only observes differences between stimulated, sham treated, and control animals in response to stimulation for a limited number of hours each day. From a translational neuroscience perspective, it would have been beneficial to closely mimic the clinical DBS protocol where chronic stimulation is administered 24 h/day (Lozano et al., 2008; Mayberg et al., 2005; Kennedy et al., 2011). Unfortunately mimicking this scenario was not feasible, and we thus opted to stimulate the mice for a limited number of hours; a paradigm that has shown to induce anti-depressant effects in rats in previous work from our group (Hamani et al., 2010). To that end it is unclear the extent to which neuroanatomical plasticity may be linked to the anti-depressant-like effects previously reported clinically. Another way to test the association between neuroanatomical remodeling would have been to administer a forced swim test as previously done by our group (Hamani et al., 2010, 2012) in order to provide putative associations between the observed result and behavioural changes. As a result associations between our results (and those of many preclinical studies) and their possible translation to clinical practice should be considered speculative. However, given the literature reviewed above it is plausible that there is an association between neuroanatomical remodeling observed and therapeutic effects previously observed.

In summary, ours is the first study to combine MRI and histology in the context of experimental DBS. We demonstrate that volumetric changes that can be resolved using MRI do indeed accompany stimulation, and are further correlated with specific neuroanatomical processes, especially those related to blood flow and neuronal synaptic connectivity. Our findings suggest the exciting possibility of compensatory or even neuroregenerative mechanisms initiated by electrical stimulation, and the possible role of the micro-lesion in acute post-operative response in depressed patients prior to the initiation of active stimulation. Further work is needed to elucidate the extent, time course, and patterning of neuroanatomical changes accompanying DBS for depression and other illnesses.

Acknowledgments

M.M.C. is supported by funding from the Weston Brain Institute, Michael J. Fox Foundation, Alzheimer's Society, National Sciences and Engineering Research Council of Canada, Canadian Institutes of Health

Research, and Brain Canada. M.M.C receives salary support from the Fonds de recherches Santé Québec (Junior 1 Scholar Program). T.S. is supported by a Canadian Institutes of Health Research (CIHR) fellowship award. J.P.L is funded by the CIHR and Brain Canada.

Disclosures

M.M.C: none, C.H.: none, A. M-C.: none, J.E.: none, C.L.: none, J.N.N.: none, T.S.: none, A.M.L.: is a consultant to Medtronic, St. Jude, and Boston Scientific. A.M.L. serves on the scientific advisory board of Ceregene, Codman, Neurophage, Aleva and Alcyone Life Sciences. A.M.L. is a co-founder of Functional Neuromodulation Inc. and holds intellectual property in the field of Deep Brain Stimulation. P.W.F.: none, J.P.L.: none.

Appendix A. Supplementary data

Supplementary data to this article can be found online at http://dx.doi.org/10.1016/j.neuroimage.2015.10.049.

References

Avants, B.B., Epstein, C.L., Grossman, M., Gee, J.C., 2008. Symmetric diffeomorphic image registration with cross-correlation: evaluating automated labeling of elderly and neurodegenerative brain. Med. Image Anal. 12, 26–41.

Borden, A., Wallon, D., Lefaucheur, R., Derrey, S., Fetter, D., Verin, M., Maltete, D., 2014. Does early verbal fluency decline after STN implantation predict long-term cognitive outcome after STN-DBS in Parkinson's disease? J. Neurol. Sci. 346, 299–302.

Carpenter, A.E., Jones, T.R., Lamprecht, M.R., Clarke, C., Kang, I.H., Friman, O., Guertin, D.A., Chang, J.H., Lindquist, R.A., Moffat, J., et al., 2006. Cell Profiler: image analysis software for identifying and quantifying cell phenotypes. Genome Biol. 7, R100.

Cersosimo, M.G., Raina, G.B., Benarroch, E.E., Piedimonte, F., Aleman, G.G., Micheli, F.E., 2009. Micro lesion effect of the globus pallidus internus and outcome with deep brain stimulation in patients with Parkinson disease and dystonia. Mov. Disord. 24, 1488–1493.

Chen, F., Madsen, T.M., Wegener, G., Nyengaard, J.R., 2008. Changes in rat hippocampal CA1 synapses following imipramine treatment. Hippocampus 18, 631–639.

Chen, F., Madsen, T.M., Wegener, G., Nyengaard, J.R., 2009. Repeated electroconvulsive seizures increase the total number of synapses in adult male rat hippocampus. Eur. Neuropsychopharmacol. 19, 329–338.

Chung, M.K., Worsley, K.J., Paus, T., Cherif, C., Collins, D.L., Giedd, J.N., Rapoport, J.L., Evans, A.C., 2001. A unified statistical approach to deformation-based morphometry. NeuroImage 14, 595–606.

Collins, D.L., Neelin, P., Peters, T.M., Evans, A.C., 1994. Automatic 3D intersubject registration of MR volumetric data in standardized Talairach space. J. Comput. Assist. Tomogr. 18, 192–205.

Conwell, Y., Brent, D., 1995. Suicide and aging. I: patterns of psychiatric diagnosis. Int. Psychogeriatr. 7, 149–164.

Dorr, A.E., Lerch, J.P., Spring, S., Kabani, N., Henkelman, R.M., 2008. High resolution three-dimensional brain atlas using an average magnetic resonance image of 40 adult C57Bl/6 J mice. NeuroImage 42, 60–69.

Franklin, K.B.J., Paxinos, G., 2004. The Mouse Brain in Stereotaxic Coordinates. Elsevier Science, London, UK.

Genovese, C.R., Lazar, N.A., Nichols, T., 2002. Thresholding of statistical maps in functional neuroimaging using the false discovery rate. NeuroImage 15, 870–878.

Granziera, C., Pollo, C., Russmann, H., Staedler, C., Ghika, J., Villemure, J.G., Burkhard, P.R., Vingerhoets, F.J., 2008. Sub-acute delayed failure of subthalamic DBS in Parkinson's disease: the role of micro-lesion effect. Parkinsonism Relat. Disord. 14, 109–113.

Hamani, C., Diwan, M., Macedo, C.E., Brandao, M.L., Shumake, J., Gonzalez-Lima, F., Raymond, R., Lozano, A.M., Fletcher, P.J., Nobrega, J.N., 2010. Antidepressant-like effects of medial prefrontal cortex deep brain stimulation in rats. Biol. Psychiatry 67, 117–124.

Hamani, C., Stone, S.S., Garten, A., Lozano, A.M., Winocur, G., 2011. Memory rescue and enhanced neurogenesis following electrical stimulation of the anterior thalamus in rats treated with corticosterone. Exp. Neurol. 232, 100–104.

Hamani, C., Machado, D.C., Hipolide, D.C., Dubiela, F.P., Suchecki, D., Macedo, C.E., Tescarollo, F., Martins, U., Covolan, L., Nobrega, J.N., 2012. Deep brain stimulation reverses anhedonic-like behavior in a chronic model of depression: role of serotonin and brain derived neurotrophic factor. Biol. Psychiatry 71, 30–35.

Hotta, H., Masamoto, K., Uchida, S., Sekiguchi, Y., Takuwa, H., Kawaguchi, H., Shigemoto, K., Sudo, R., Tanishita, K., Ito, H., et al., 2013. Layer-specific dilation of penetrating arteries induced by stimulation of the nucleus basalis of Meynert in the mouse frontal cortex. J. Cereb. Blood Flow Metab. 33, 1440–1447.

Kaae, S.S., Chen, F., Wegener, G., Madsen, T.M., Nyengaard, J.R., 2012. Quantitative hippocampal structural changes following electroconvulsive seizure treatment in a rat model of depression. Synapse 66, 667–676.

Kennedy, S.H., Giacobbe, P., Rizvi, S.J., Placenza, F.M., Nishikawa, Y., Mayberg, H.S., Lozano, A.M., 2011. Deep Brain Stimulation for Treatment-Resistant Depression: Follow-Up After 3 to 6 Years. Am. J. Psychiatry 168, 502–510.

Laxton, A.W., Tang-Wai, D.F., McAndrews, M.P., Zumsteg, D., Wennberg, R., Keren, R., Wherrett, J., Naglie, G., Hamani, C., Smith, G.S., et al., 2010. A phase I trial of deep brain stimulation of memory circuits in Alzheimer's disease. Ann. Neurol. 68, 521–534.

Le Goff, F., Derrey, S., Lefaucheur, R., Borden, A., Fetter, D., Jan, M., Wallon, D., Maltete, D., 2014. Decline in verbal fluency after subthalamic nucleus deep brain stimulation in Parkinson's disease: a microlesion effect of the electrode trajectory? J. Park. Dis. 5, 95–104.

Lerch, J.P., Carroll, J.B., Spring, S., Bertram, L.N., Schwab, C., Hayden, M.R., Henkelman, R.M., 2008. Automated deformation analysis in the YAC128 Huntington disease mouse model. NeuroImage 39, 32–39.

Lerch, J.P., Yiu, A.P., Martinez-Canabal, A., Pekar, T., Bohbot, V.D., Frankland, P.W., Henkelman, R.M., Josselyn, S.A., Sled, J.G., 2011. Maze training in mice induces MRI-detectable brain shape changes specific to the type of learning. NeuroImage 54, 2086–2095.

Limousin, P., Pollak, P., Benazzouz, A., Hoffmann, D., Le Bas, J.F., Broussolle, E., Perret, J.E., Benabid, A.L., 1995. Effect of parkinsonian signs and symptoms of bilateral subthalamic nucleus stimulation. Lancet 345, 91–95.

Lipsman, N., Woodside, D.B., Giacobbe, P., Hamani, C., Carter, J.C., Norwood, S.J., Sutandar, K., Staab, R., Elias, G., Lyman, C.H., et al., 2013. Subcallosal cingulate deep brain stimulation for treatment-refractory anorexia nervosa: a phase 1 pilot trial. Lancet 381, 1361–1370.

Lozano, A.M., Lipsman, N., 2013. Probing and regulating dysfunctional circuits using deep brain stimulation. Neuron 77, 406–424.

Lozano, A.M., Mayberg, H.S., Giacobbe, P., Hamani, C., Craddock, R.C., Kennedy, S.H., 2008. Subcallosal cingulate gyrus deep brain stimulation for treatment-resistant depression. Biol. Psychiatry 64, 461–467.

Maltete, D., Derrey, S., Chastan, N., Debono, B., Gerardin, E., Freger, P., Mihout, B., Menard, J.F., Hannequin, D., 2008. Microsubthalamotomy: an immediate predictor of long-term subthalamic stimulation efficacy in Parkinson disease. Mov. Disord. 23, 1047–1050.

Maltete, D., Chastan, N., Derrey, S., Debono, B., Gerardin, E., Lefaucheur, R., Mihout, B., Hannequin, D., 2009. Microsubthalamotomy effect at day 3: screening for determinants. Mov. Disord. 24, 286–289.

Mayberg, H.S., Lozano, A.M., Voon, V., McNeely, H.E., Seminowicz, D., Hamani, C., Schwalb, J.M., Kennedy, S.H., 2005. Deep brain stimulation for treatment-resistant depression. Neuron 45, 651–660.

McKinnon, M.C., Yucel, K., Nazarov, A., MacQueen, G.M., 2009. A meta-analysis examining clinical predictors of hippocampal volume in patients with major depressive disorder. J. Psychiatry Neurosci. 34, 41–54.

Needels, D.L., Nieto-Sampedro, M., Whittemore, S.R., Cotman, C.W., 1985. Neuronotrophic activity for ciliary ganglion neurons. Induction following injury to the brain of neonatal, adult, and aged rats. Brain Res. 350, 275–284.

Needels, D.L., Nieto-Sampedro, M., Cotman, C.W., 1986. Induction of a neurite-promoting factor in rat brain following injury or deafferentation. Neuroscience 18, 517–526.

Nieman, B.J., Bishop, J., Dazai, J., Bock, N.A., Lerch, J.P., Feintuch, A., Chen, X.J., Sled, J.G., Henkelman, R.M., 2007. MR technology for biological studies in mice. NMR Biomed. 20, 291–303.

Nordanskog, P., Dahlstrand, U., Larsson, M.R., Larsson, E.M., Knutsson, L., Johanson, A., 2010. Increase in hippocampal volume after electroconvulsive therapy in patients with depression: a volumetric magnetic resonance imaging study. J. ECT 26, 62–67.

Oh, S.W., Harris, J.A., Ng, L., Winslow, B., Cain, N., Mihalas, S., Wang, Q., Lau, C., Kuan, L., Henry, A.M., et al., 2014. A mesoscale connectome of the mouse brain. Nature 508, 207–214.

Pinheiro, J.C., Bates, D.M., 2000. Mixed-effects Models in S and S-PLUS. Springer Verlag.

Sankar, T., Chakravarty, M.M., Bescos, A., Lara, M., Obuchi, T., Laxton, A.W., McAndrews, M.P., Tang Wai, D., Workman, C.I., Smith, G.S., et al., 2015. Deep Brain Stimulation influences brain structure in Alzheimer's Disease. Brain Stimul. http://dx.doi.org/10.1016/j.brs.2014.11.020.

Scholz, J., Allemang-Grand, R., Dazai, J., Lerch, J.P., 2015. Environmental enrichment is associated with rapid volumetric brain changes in adult mice. NeuroImage 109C, 190–198.

Shah, D.B., Pesiridou, A., Baltuch, G.H., Malone, D.A., O'Reardon, J.P., 2008. Functional neurosurgery in the treatment of severe obsessive compulsive disorder and major depression: overview of disease circuits and therapeutic targeting for the clinician. Psychiatry (Edgmont) 5, 24–33.

Song, S., Song, S., Cao, C., Lin, X., Li, K., Sava, V., Sanchez-Ramos, J., 2013. Hippocampal neurogenesis and the brain repair response to brief stereotaxic insertion of a microneedle. Stem Cells Int. 2013, 205878.

Stagg, C.J., Lin, R.L., Mezue, M., Segerdahl, A., Kong, Y., Xie, J., Tracey, I., 2013. Widespread modulation of cerebral perfusion induced during and after transcranial direct current stimulation applied to the left dorsolateral prefrontal cortex. J. Neurosci. 33, 11425–11431.

Stone, S.S., Teixeira, C.M., Devito, L.M., Zaslavsky, K., Josselyn, S.A., Lozano, A.M., Frankland, P.W., 2011. Stimulation of entorhinal cortex promotes adult neurogenesis and facilitates spatial memory. J. Neurosci. 31, 13469–13484.

van Eede, M.C., Scholz, J., Chakravarty, M.M., Henkelman, R.M., Lerch, J.P., 2013. Mapping registration sensitivity in MR mouse brain images. NeuroImage 82, 226–236.

Venna, V.R., Deplanque, D., Allet, C., Belarbi, K., Hamdane, M., Bordet, R., 2009. PUFA induce antidepressant-like effects in parallel to structural and molecular changes in the hippocampus. Psychoneuroendocrinology 34, 199–211.

Willard, S.L., Riddle, D.R., Forbes, M.E., Shively, C.A., 2013. Cell number and neuropil alterations in subregions of the anterior hippocampus in a female monkey model of depression. Biol. Psychiatry 74, 890–897.

Wyckhuys, T., Staelens, S., Van Nieuwenhuyse, B., Deleye, S., Hallez, H., Vonck, K., Raedt, R., Wadman, W., Boon, P., 2010. Hippocampal deep brain stimulation induces decreased rCBF in the hippocampal formation of the rat. NeuroImage 52, 55–61.